Numerical Study of the Influence of Rim Design on the Aerodynamics of an Isolated Wheel

Huihui Zhai and Haichao Zhou

Abstract Wheel and tire contribute up to 25% of the total aerodynamic drag of passenger cars. Under the same tire mounted on the wheel, the rim holes induce air flow and result in complex flow separation in a highly unsteady regime. To have a clearer understanding of the flow mechanisms and assign sensitivity of rim parameters. The effect of rim spoke design parameters on the aerodynamics of an isolated wheel had been investigated with unsteady CFD simulation. Four design variables, the angle A, radius R1, and R2, and chord length L, which characterized the rim spoke are proposed, and the Latin hypercube sampling is used to conduct the design of the experiment (DOE). Based on the simulation results of different rim designs, the Kriging model and adaptive simulated annealing algorithm are selected to obtain the optimum parameters. The results show that the aerodynamic characteristics are very sensitive to the selected four design variables, the optimized rim changes the flow state, and the drag coefficient of the Ahmed body mounted with the optimized wheel decreased by 4.7%.

Keywords Aerodynamic drag · Isolated wheel · Numerical simulation · DOE · Optimization analysis

1 Introduction

1.1 A Subsection Sample

Due to global warming, governments and manufacturers have been taking an increasing number of active steps to reduce CO_2 emissions. One effective measure for reducing CO_2 emissions is to decrease the vehicle's aerodynamic drag. It is

H. Zhai
Institute of Electrical and Information Engineering, Zhenjiang College, Zhenjiang 212028, China

H. Zhou (✉)
School of Automotive and Traffic Engineering, Jiangsu University, Zhenjiang 212013, China
e-mail: haichaozhou999@163.com

S. Li (ed.), *Computational and Experimental Simulations in Engineering*, Mechanisms and Machine Science 146, https://doi.org/10.1007/978-3-031-44947-5_103

reported that a 5% reduction in aerodynamic drag of a car could result in a reduction of 1.5 g/km of CO_2. Therefore, engineers and scholars have made largely efforts to improve the aerodynamic performance of vehicles. Lots of studies have shown that particularly the wheels have a considerable influence on the aerodynamic properties and can actually contribute up to 25% of the total drag on modern vehicles [1]. The aerodynamic drag has a direct relationship with the flow field around the car, and the high contribution of wheel on drag is due to the strong interactions between wheel wake and the vehicle underbody through pressure modifications. Hence, when the body shape optimization reaches its limits, wheels aerodynamics is becoming prominent and as a major concern in order to reduce fuel consumption. Meanwhile, reduce wheel aerodynamic drag is benefit to enlarge the range of EV. Consequently, over the past two decades, wheel aerodynamics has been the focus of numerous studies and optimization efforts in academia and in industry [2–4].

Frackell [5] carried out the first experiment work about an isolated wheel in realistic conditions, and the results show that the pressure distribution measured on the wheel surface highlighted two main specificities of the flow, the wheel rotation moved forward stagnation point ~ 15° down towards the front contact patch at the ground, the jetting-vortices effects appears at either side of the contact patch. Brandt et al. [6] designed several different types of wheels, and the effects of certain rim parameters on flow filed and drag is studied using CFD, and put forward a conclusion that the drag is a linear relationship with the cover area of wheel spoke. Fang et al. [7] investigated the influence of rim cover area on the drag using wind tunnel test, they found that the full cover wheel has a lowest drag coefficient. Fu et al. [8] studied the aerodynamic characteristics of wheel and car using different wheel opening area and design location, and it was shown that under the same opening area condition, increasing the number of openings can improve the aerodynamic performances.

Despite the known potential in the modification of the wheel to reduce drag, the understanding of the flow phenomenon and their interaction with surrounding parts still offers considerable room for improvement of wheel aerodynamics. Elofsson and Bannister [9] presented a schematic picture of the near-wake structures including the two jetting-vortices, two vortices downstream of the upper wheel boundary separation. Saddington et al. [10] analyzed the flow field around the wheel using the Laser doppler anemometry LDV system, and the results show that the upper vortices appeared to be weaker and to merge with the jetting-vortices within on diameter downstream behind the wheel axis. The use of computational fluid dynamics added a further insight into the understanding of wheel flow field and aerodynamics. The simulation with isolated wheel tended essentially to demonstrate the CFD ability to capture specific flow features and to better understanding the vortex dynamics and their impact on aerodynamic drag.

Although the effect of wheel design and the main flow features has already been studied both experimentally and numerically, to the author's knowledge, few studies were conducted with the wheel spoke opening optimize design to reduce drag. The present study aims to investigate the influence of spoke opening design parameters on wheel drag. After then, the kriging model and ASA method are used to optimize

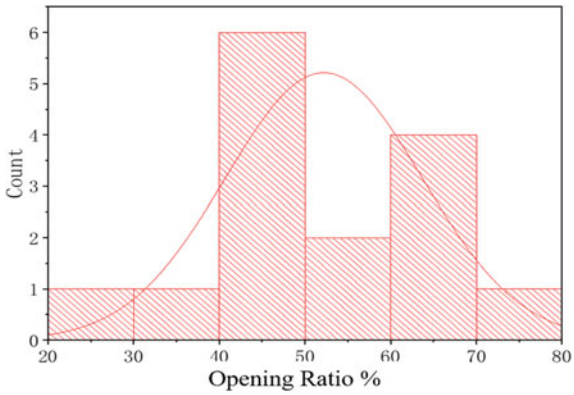

Fig. 1 The opening ration distribution

the opening design for the reducing drag as much as possible. The difference of flow field between the original design and the optimized design is also discussed.

2 Wheel Geometry

In order to obtain the universal effects law of the spoke opening on the wheel aerodynamics, the opening ratio of 15 type popular car models in the market is investigated and analyzed, and the opening ratio of these selected car with five spoke holes is mainly concentrated in the 50–55%, as shown in Fig. 1. Thus the wheel with five holes is chosen as research object in this work, and the opening ratio is 52%. The wheel has diameter of 150 mm, the width is 50 mm. All the details size of the wheel is listed in the Fig. 2. Due to the pressure peak and jetting effect at the edges of the wheel, the contact patch region of the wheel with the ground is modelled as a convex plate with the height of 0.2 mm and length of 25 mm for computational analysis since it affects the mesh quality and the wake airflow behaviors.

3 Grid Description and Computational Method

Based on the length L, width W and height H of the wheel, the domain boundary was designed to be 20 L long, 10 W width and 5 H height, as showed in Fig. 3. The wheel was placed middle in the width direction, with 7 L clearance to the inlet. The blockage ratio is about 2%. The grid was generated using the commercial software Hypermesh to generate the volume mesh and boundary layer cell. A cylindrical shaped volumetric control around the wheel and a rectangular shaped volumetric control at the wake are carried out to better capture the flow features in these regions.

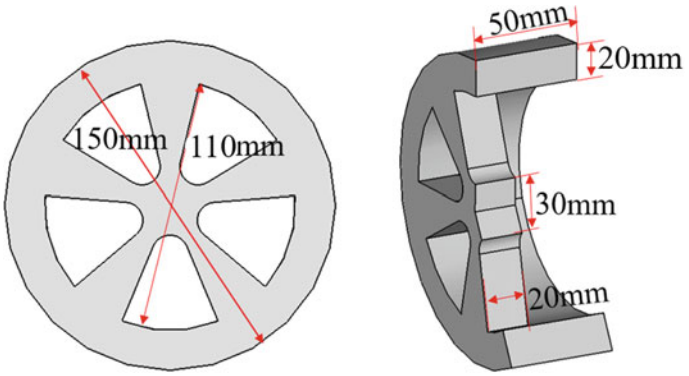

Fig. 2 A wheel with five hole

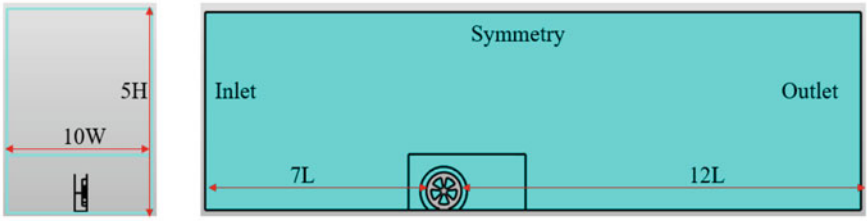

(a) Computational domain sizes

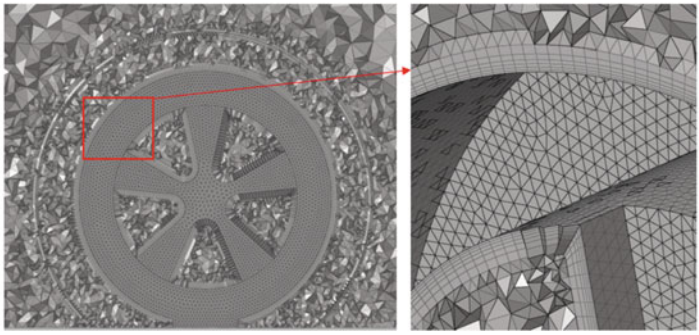

(b) Local mesh refinement

Fig. 3 Computational domain sizes and grids

The grids generated were then solved with the commercial software Ansys Fluent 18.2 to take advantage of available parallel computing resources. The simulation process were run until the flow reached an acceptable convergence judged by two criteria. Firstly, a steady state calculation was run until the flow has reached a full convergence such that the normalized residuals of all transported quantities dropped at least three order of magnitude and was steady. Then the steady simulation results were used for initializing the computational domain for the unsteady computation.

Table 1 Computational domain grid size

	Surface sizes	Ratio	Number of layers	Frist size of layer
Domain	10–50	–	–	–
Ground	0.8–10	1.3	5	0.05
Wheel	0.8–2	1.3	5	0.05

Table 2 Drag coefficients among three grid schemes

Schemes	Coarse mesh	Medium mesh	Fine mesh
C_d	0.963	0.941	0.934

The DES model utilized the SST turbulence model, it was chosen because of its common use in the industry to model vehicle flows [11]. The second-order, upwind discretization scheme was used for the pressure, momentum, turbulent kinetic energy and specific dissipation terms of the Navier Stokes equation for the unsteady RANS and DES methods. The unsteady simulation was computed with a 0.001 s time step, and each time step including 10 iterative steps. The total computations time is 2 s.

The inlet was set to a constant velocity of 10 m/s, and the outlet was set to a atmospheric conditions, the floor was modelled as a static ground wall. The surface of wheel was set as a rotating boundary with 21.9 r/s. The top is symmetry plane. The other boundaries of the computation domain were set to be zero shear walls. To investigate the different mesh resolution sensitivity, four grids were generated, named as coarse mesh, medium mesh and fine mesh, and the details of the three mesh are shown in Fig. 3. The main difference of the three mesh schemes is the mesh size of the model surfaces and boundary layers, as shown in Table 1.

All the drag coefficients of the three mesh schemes are shown in Table 2, and it can be found that as the number of grid increases, the drag coefficients decrease. The error between the medium and the fine is only 0.74%. The medium grid is selected to conduct the following simulations. This grid has a y + value of < 2 all around the wheel surface, as shown in Fig. 4.

4 Parameter Optimization of the Rim Spoke Hole

4.1 Parameters Selection and DOE

The structure of spoke holes has important influences on aerodynamic drag because in influences air movement. Under the same area of the rim hole, keeping the diameter of wheel fix at 75 mm, the five characteristic parameters of rim spoke, named as fillet angle α, inside arc radius R1 and outside arc radius R2; the same arc tangent lines L1 and L2, as shown in Fig. 5. In the original spoke hole design, the fillet angle α = 0.384 rad, inside arc radius R1 and outside arc radius R2 are 8 mm and 25 mm,

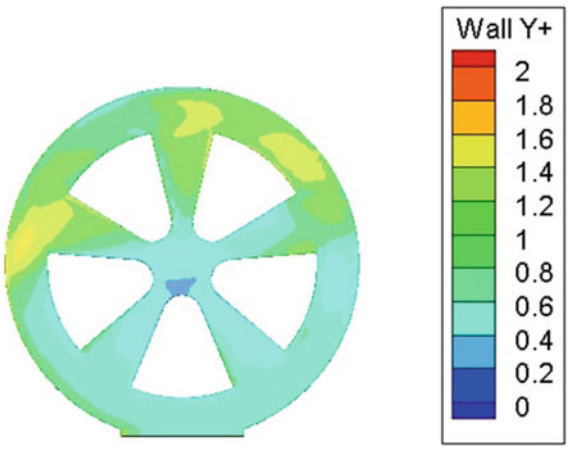

Fig. 4 Y^+ values distribution around wheel surface

respectively; the same arc tangent lines L1 and L2 are the same as 35.69 mm. To investigate the different rim parameters on the aerodynamic drag of the wheel under the same area of rim hole, the parameters variables were set to following values: $\alpha \in (0.2618, 0.5235)rad$, $R_2 \in (41.5824, 58.6799)mm$ and the other variables are determined according to the Eqs. 1–3.

$$S = \alpha \cdot R_2^2 - 20.91^2 \cdot \sin(\alpha) \cdot \cos(\alpha) + \frac{(\pi - \alpha)}{2} \cdot 20.91^2 \cdot (\sin(\alpha))^2 \quad (1)$$

$$R_1 = 20.91 \cdot \sin(\alpha) \quad (2)$$

$$L_1 = L_2 = R_2 - 20.91 \cdot \cos(\alpha) \quad (3)$$

Of many experiments methods to generate test schemes, the Optimal Latin Hypercube design method can ensure that the factor level combination of each factor is optimized rather randomly or evenly divided. Thus, the factors and levels selected for the OLH design and the response numerical simulation are listed in the Table 3. The design of the schemes 7, 11 and 16 were presented in the Fig. 6. The main effects of the parameter variables on the aerodynamic drag coefficient of the wheel were shown in the Fig. 7, and it can be seen that the fillet angle α has the greatest impact on drag coefficient, followed by the outside arc radius R_2, and the arc tangent lines L_1 and L_2 has minimal impact.

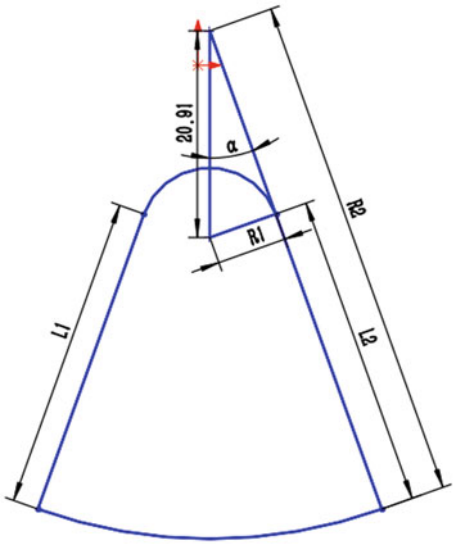

Fig. 5 Schematic diagram of a single spoke hole

Table 3 Test schemes and calculation results

No	L_1, L_2/mm	R_1/mm	R_2/mm	α	C_d
1	30.6066	9.6906	42.1299	0.482	0.957
2	29.4051	10.2053	47.6498	0.51	0.951
3	29.9652	7.5985	58.0359	0.372	0.960
4	31.7047	7.0503	60.1428	0.344	0.959
5	27.1245	8.6576	52.3857	0.427	0.891
6	28.434	8.1408	54.1919	0.4	0.919
7	46.8267	5.4106	67.0194	0.2618	0.940
8	45.1861	5.6968	65.2999	0.276	0.943
9	42.4004	6.2377	62.3531	0.303	0.956
10	31.8865	9.187	50.6646	0.455	0.951
11	34.2891	7.8704	55.1935	0.386	0.950
12	41.1032	6.5165	60.9666	0.317	0.954
13	34.1555	8.3904	53.3028	0.413	0.885
14	32.6025	8.9232	51.5074	0.441	0.946
15	37.7722	7.3251	57.3518	0.358	0.951
16	28.863	10.4525	46.9672	0.5236	0.968
17	39.8928	6.7939	59.663	0.331	0.950
18	43.7944	5.9578	63.8325	0.289	0.938
19	29.9908	9.9489	48.3766	0.496	0.950
20	31.2544	9.4303	49.9115	0.468	0.957

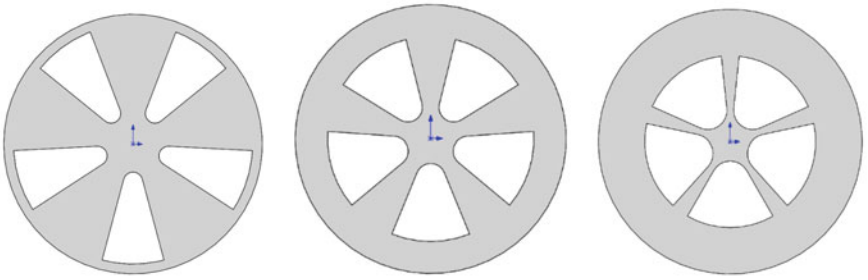

(a) Scheme 7 (b) Scheme 11 (c) Scheme 16

Fig. 6 Geometric models of some typical schemes

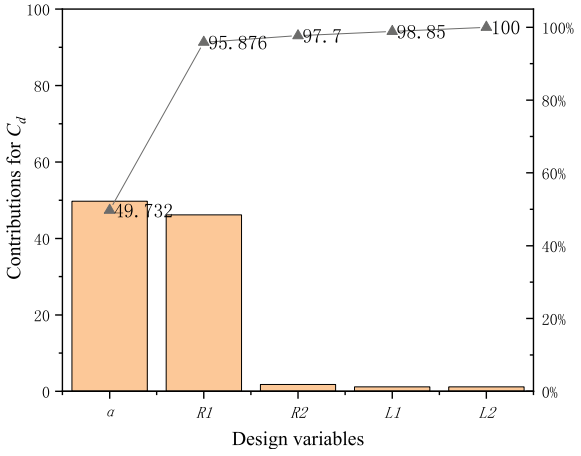

Fig. 7 Contribution of different design variables for C_d

4.2 Surrogate Model and Optimization

The Kriging surrogate model is a method of curve interpolation and response surface approximation, which have proved to be effective for approximate evaluation of design points. Based on the computational results shown Table 4, the surrogate model of this study achieved high accuracy in interpolating the 20 experimental schemes, and the correlation coefficient R^2 were selected to evaluate the accuracy of the built Kriging surrogate model. Figure 8 shows the forecast accuracy between the simulation results and predict results, and the R^2 is about 0.98. It means that the established surrogate model has enough accuracy to realize the parameters optimization of the rim spoke hole.

The SA algorithm provided in the Insight software is selected to obtain the globe optimal solution from the design valuables. For the SA algorithm, the objective function is to minimize the wheel drag coefficient, and the constraint conditions were set as $\alpha \in (0.2618, 0.5235)rad$, $R_2 \in (41.5824, 58.6799)mm$; $R_1 \in$

Table 4 Comparison of aerodynamic drag coefficients before and after optimization

	L_1, L_2/mm	R_1/mm	R_2/mm	a/rad	C_d
Original	35.6863	8	55	0.384	0.934
Optimized	33.9051	8.4729	53.0161	0.393	0.883

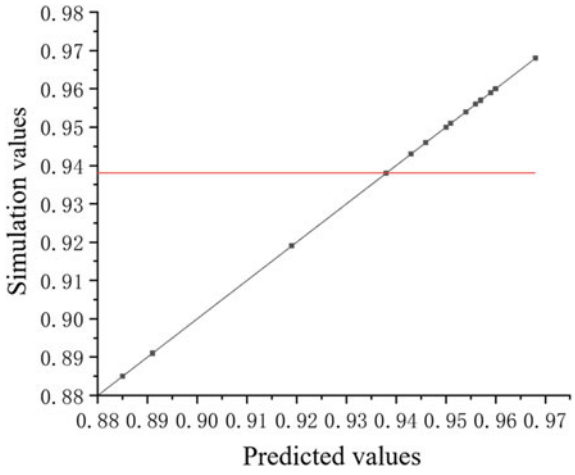

Fig. 8 Kriging surrogate model accuracy

Table 5 Before and after optimization of vehicle aerodynamic drag coefficient

	C_d of the model	C_d of the front wheel	C_d of the rear wheel
Original model	0.402	0.0364	0.0246
Optimized model	0.384	0.0312	0.0210

$(5.4106, 10.4525)mm$, $L_1 \in (27.1245, 46.8267)mm$ after the 382 iterations, the optimal feasible solutions is listed in the Table 5, and the sizes of the original and optimized wheel are presented in Fig. 9. According to the optimized parameters, a new wheel model was established and analyzed, and the wheel drag coefficient is 0.883, and it decreased by 5.7% compared with the original drag coefficient of 0.934.

5 Results Analysis and Discussion

5.1 Flow Field

To reveal the influence of the wheel spoke before and after optimized on the flow field and aerodynamic drag, three vertical sections and a longitudinal section are used to analyze the difference of flow field information, as shown in Fig. 10.

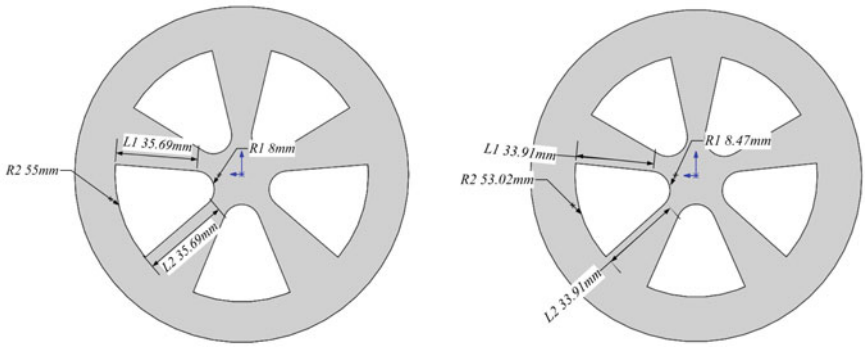

(a) Original wheel (b) Optimized wheel

Fig. 9 Comparison of the opening shapes of the front spokes

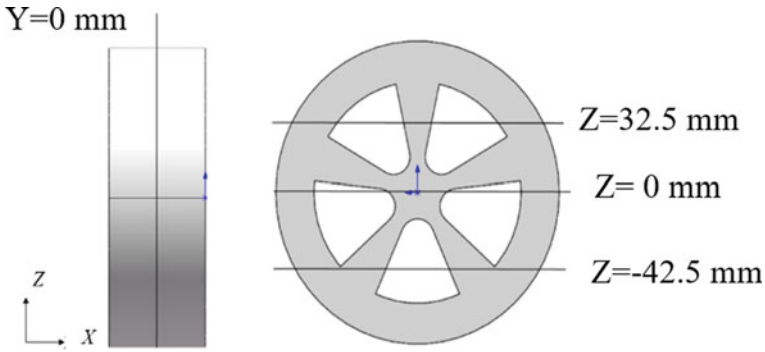

Fig. 10 Four different sections

The pressure drag is the major component of the aerodynamic drag. Figure 11 depicts the pressure contour in the Y = 0 section of the wheel. It can be seen that the air pressure around the front of wheel has barely changes, but the pressure in the rear has obvious changes with the pressure values increasing. The change of pressure magnitude means the pressure drag decrease and the wheel drag is also reduced.

The compassion of the turbulent kinetic energy before and after optimization is shown in Fig. 12. Due to the increasing of the inside arc radius R1, the air flow uplift and passes through the spoke hole, this make the TKE nearby the ground decrease, which implies that air flow around the contact patch was more stable. The more air flow passes through the hole and move into the wake region, and the larger TKE boundary faraway wheel rear surface, the air flow energy consumption was lower, and the aerodynamic performance was improved.

Figure 13 shows the streamlines and vorticity inside the wheel cavity on the different Z-direction sections. Due to the block effect of wheel, the air flow first

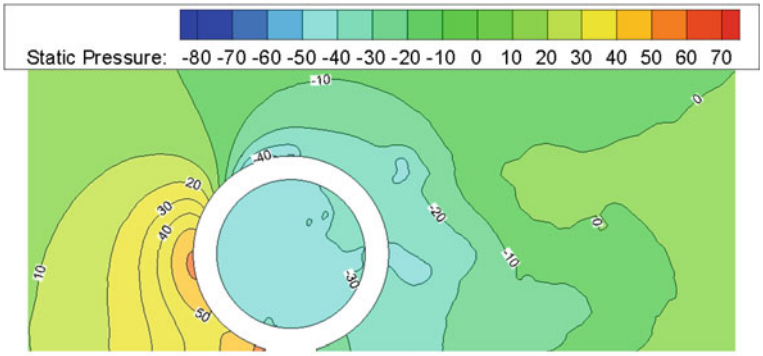

(a) The original wheel

(b) The optimized wheel

Fig. 11 Pressure of longitudinal plane in wheel before and after optimization

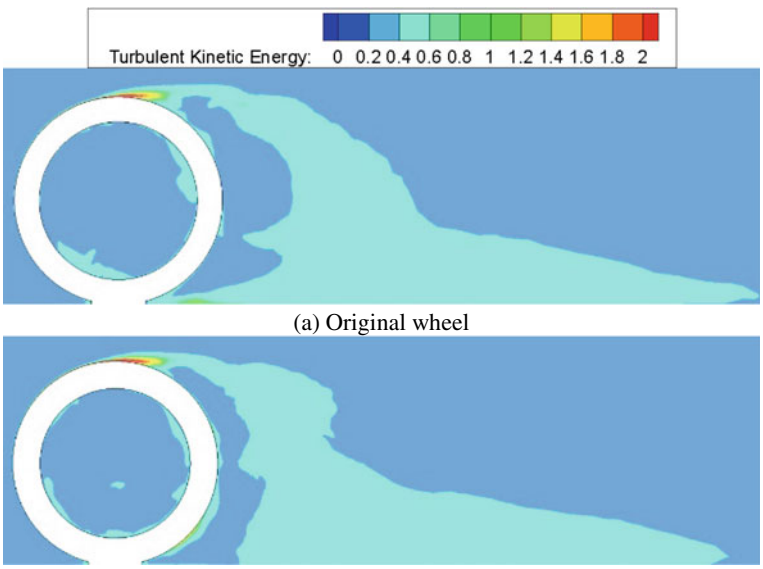

(a) Original wheel

(b) Optimized wheel

Fig. 12 The turbulent kinetic energy at the rear of the wheel

separates at the front edge of wheel to form two streams and propagate downstream. Because of the existence of the wheel cavity, the low velocity airflow has unsteady flow characters, and lot of flow vortex appear. Once airflow impact the rear edges of the wheel cavity, the airflow velocity around inside edge will decreases and vorticity increase; under the driving effect of the high-speed from the front edge, the whole airflow vorticity nearby the inside zone is larger than that of the outside zone. Owing to the ventilation capacity of the spoke hole improves, the vorticity distribution inside cavity of the optimized wheel is smaller than that of the original wheel. It can be seen from the Fig. 13a that the flow field around the outside zone of wheel have little changes, while there are significant differences nearby the inside zone of wheel. The optimized rim forces the vortex core backward and the vorticity in the vortex central region decreased. However, the vorticity intensity inside the optimized wheel cavity is higher than that of the original wheel. Figure 13b shows the comparison of flow field at the $Z = 0$ mm section. Although the flow field behind the wheel is similar, the optimized wheel has a wider hole to better direct the airflow into the wheel cavity, and a bigger streamline vortex region appears nearby the inside edge of the rim. It can be seen from the streamline in Fig. 13c that there are a couple of vortexes behind the optimized wheel, which is not exist for the original wheel. The vortices magnitude in the optimized wheel cavity is relatively uniform, and it means that airflow is steady state and flow energy loss decrease. Besides, the regions of the higher vorticity in the optimized wheel are less than of that in the original wheel.

5.2 Aerodynamic Characteristics of Ahmed Body with Wheel

According to the research method provided in the Ref [12, 13], the aerodynamic drag of an Ahmed body mounted with the original and optimized wheel is studied, and Fig. 14 shows the comparison of the pressure coefficient distribution of the body surfaces. In Fig. 14, compared with the original wheel, the pressure coefficient around the front wheel increase and the rear wheel decreases, it means that the rim spoke hole has a directly influence on the airflow movement around the wheel; for the back surface of car body, the pressure coefficient of the slant rear surface reduces, but with the help of the change of the airflow state in the under-body gap, it caused a significant increase in the pressure coefficient of the vertical rear surface. The drag coefficients are shown in Table 5. It can see that drag coefficient of the Ahmed body reducing 4.7%, and the front wheel and the rear wheel is decreased by 16.7% and 17.1%, respectively. It can be concluded that improving the geometric characteristics of the wheel aerodynamic shape is one of the effective measures to improve automotive aerodynamic characteristics and reduce drag.

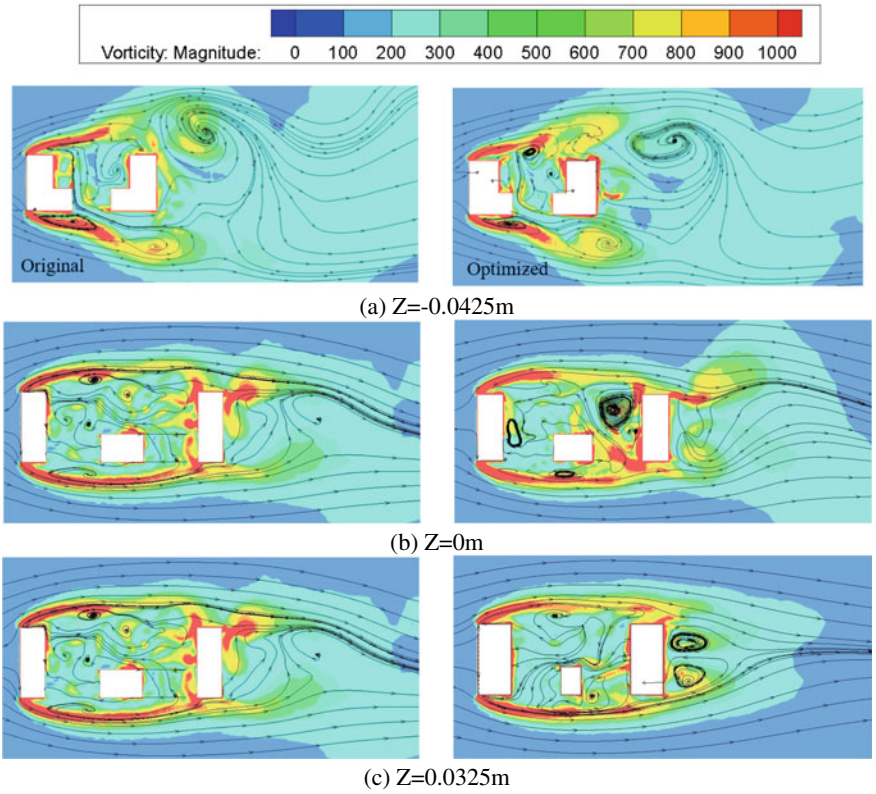

(a) Z=-0.0425m

(b) Z=0m

(c) Z=0.0325m

Fig. 13 Comparison of vorticity of different sections

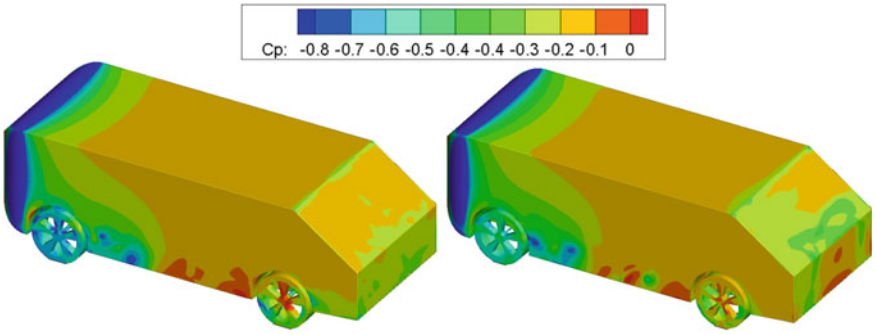

(a) Ahmed body with original wheel (b) Ahmed body with optimized wheel

Fig. 14 Surface pressure coefficient of the Ahmed body

6 Conclusion

This study conducted a numerical investigation to the influence of rim design on the aerodynamics of an isolated wheel. The main conclusions are enumerated as follows:

(1) The aerodynamic characteristics of an isolated wheel was studied using numerical simulation, and the four design parameters of wheel spoke holes, the angle α, radius R_1, and R_2, and chord length L, are selected as variables, and the drag coefficient as object. It is found that the angle α has the greatest impact on drag coefficient, followed by the outside arc radius R_2, and the arc tangent lines L_1 and L_2 has minimal influence.
(2) Based on the integrated application of Kriging surrogate model and adaptive simulated annealing algorithm, the optimal design parameters of four parameter of spoke hole are obtained. Through comparison and analysis of the differences of flow field, the optimized wheel influences the airflow state inside the wheel cavity, and reducing the flow instability in the rear zone of the wheel, the drag coefficient of the isolated wheel reducing 5.7%.
(3) The aerodynamic drag of an Ahmed body mounted with the original and optimized wheel is studied, and the optimized wheel has a direct influence on the pressure coefficients around the car body, and the drag coefficient of the Ahmed body is decreased by 4.7%.

Acknowledgements This authors are pleased to acknowledge funding of the National Natural Science Foundation of China (Nos. 52072156, 51675240, and 51605198), and Postdoctoral Foundation of China (2020M682269).

References

1. Huminic, A., Huminic, G.: Aerodynamic study of a generic car model with wheels and underbody diffuser. Int. J. Autom. Technol. **18**, 397–404 (2017)
2. Zhou, H., Jiang, Z., Wang, G., et al.: Aerodynamic characteristics of isolated loaded tires with different tread patterns: experiment and simulation. Chin. J. Mech. Eng. **34**, 1–16 (2021)
3. Zhang, L., Zhou, H., Wang, G., et al.: Investigation of effects of tire contour on aerodynamic characteristics and its optimization. Proceed. Instit. Mech. Eng. D J. Autom. Eng. **236**(12), 2756–2772 (2022)
4. Jiang, F., Niu, J., Li, R., et al.: Computational fluid dynamics analysis of effect of braking plate configurations on the aerodynamic behaviors of an Ahmed car. Flow Turbul. Combust. **110**, 301–323 (2023)
5. Fackrell, J.E.: The Aerodynamic of an Isolated Tire Rotating in Contact with Ground. University of London, London (1974)
6. Brandt, A., Berg, H., Bolzon, M., et al.: The effects of wheel design on the aerodynamic drag of passenger vehicles. SAE Int. J. Adv. Curr. Pract. Mobil. **1**(662), 1279–1299 (2019)
7. Fang, J., Wang, F.L.: A study on CFD simulation and wind tunnel test on aerodynamic effects of wheel rotation and drag reduction optimization. Automot. Eng. **41**(9), 1006–1012 (2019)
8. Fu, L.M., Hu, X.J., Zhang, S.C.: Numerical simulation of influence of holes in wheel spokes on automotive external flow field. Trans. Chin. Soc. Agricult. Mach. **37**(1), 8–11 (2006)

9. Elofsson, P., Bannister, M.: Drag reduction mechanisms due to moving ground and wheel rotation in passenger cars. SAE Trans. **1**(531), 591–604 (2002)
10. Saddington, A.J., Knowles, R.D., Knowles, K.: Laser Doppler anemometry measurements in the near-wake of an isolated formula one wheel. Exper. Fluids **42**(5), 671–681 (2007)
11. Liang, H., Sun, Y., Li, T., et al.: Influence of marshalling length on aerodynamic characteristics of urban emus under crosswind. J. Appl. Fluid Mech. **16**(1), 9–20 (2022)
12. Zhou, H., Qin, R., Wang, G., et al.: Comparative analysis of the aerodynamic behavior on Ahmed body mounted with different wheel configurations. Proceed. Instit. Mech. Eng. D J. Autom. Eng. **2022**, 09544070221121877 (2022)
13. Zhou, H., Chen, Q., Qin, R., et al.: Investigation of wheelhouse shapes on the aerodynamic characteristics of a generic car model. Adv. Mech. Eng. **13**(12), 1–13 (2021)